Comparison of the Performance of the Dual-Readout Calorimeter for different absorbers

Seoyun Jang[1,*] on behalf of the Korea Dual-Readout Calorimeter R&D Collaboration

[1]Department of Physics, Yonsei University, Seoul 03722, Korea

Abstract. Future lepton collider experiments (FCC-ee and CEPC) require excellent hadronic energy resolution to exploit their advantages. The dual-readout calorimeter can satisfy this requirement by using two types of calorimeter signals, which provide complementary information about the shower development. The calorimeter design considers a range of different absorbers. We investigated the performance, including the energy resolution of EM and hadronic particles as well as shower developments, of the dual-readout calorimeter for different absorbers such as Fe, Brass, Cu, Pb, and W. In this paper, we present a performance comparison of these absorbers derived from GEANT4 simulation studies.

1 Introduction

In high-energy physics, improving the resolution of energy measurement of a hadronic shower is one of the challenging tasks. The energy resolution of hadronic particles is limited by the fact that the fraction of electromagnetic (EM) component does fluctuate. Dual-readout calorimetry [1] addresses this issue by measuring both EM and hadronic components simultaneously through two separate channels: Cherenkov and scintillation. Each channel exhibits a distinct response ratio to EM (e) and hadronic (h) particles, allows to measure fraction of EM component (f_{EM}) within the hadron shower.

To implement the dual-readout concept, one crucial decision is selecting the absorber material for the geometry. As the dual-readout calorimeter measures both EM and hadronic showers simultaneously, various factors must be considered when choosing an absorber. We investigated the performance of different absorbers for both EM and hadronic particles based on Monte Carlo (MC) simulations.

2 Simulation Setup

2.1 Geometry, Physics setup

The cuboid geometry of the dual-readout calorimeter was implemented in GEANT4 simulation [2]. The geometry consists of Cherenkov and scintillating optical fibers, which are implemented longitudinally unsegmented in absorber. Figure 1 shows the dimensions and arrangement of optical fibers, in the upstream view of the module. The fibers are arranged alternately, ensuring a uniform geometry for both channels. We selected 5 different absorbers generally used in calorimetry - Copper, Brass

---

*e-mail: seo.yun.jang@cern.ch

(Cu:Zn=7:3), Iron, Lead, and Tungsten. All modules have the same dimensions of $69.3 \times 69.3\ cm^2$ at the front and a 2.5 m depth in longitudinal direction, providing more than 10 nuclear interaction length regardless of absorber.
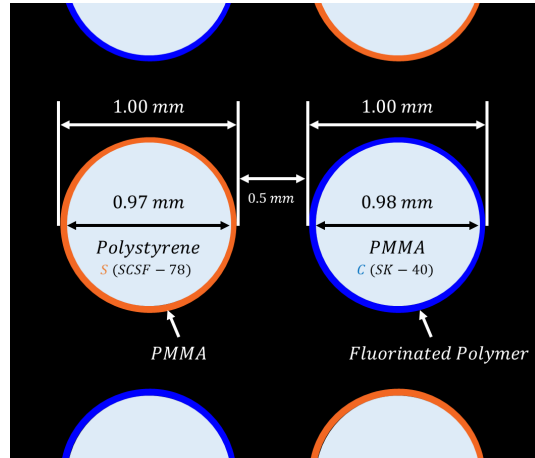

Figure 1. Zoomed view of optical fiber arrangement in upstream of the module in simulation. Used Kuraray SCSF-78 single cladding fiber for scintillation channel, and Mitsubishi Eska SK-40 clear fiber for Cherenkov channel.

The simulation setup was done in GEANT4-10.5.p01 version, using physics list FTFP-BERT. The optical physics of photons generated inside optical fibers - from the Cherenkov and scintillation light emission to propagation - were fully simulated.

Optical photons were detected with silicon photomultiplier (SiPM) attached at the end of optical fibers. The data sheet of Hamamatsu S13615-1025N SiPM [3] was used to describe SiPM in simulation. In the case of scintillating fibers, Kodak Wratten #9 yellow filters were inserted between fiber and SiPM, on purpose to decrease light attenuation effect inside fibers by filtering blue lights.
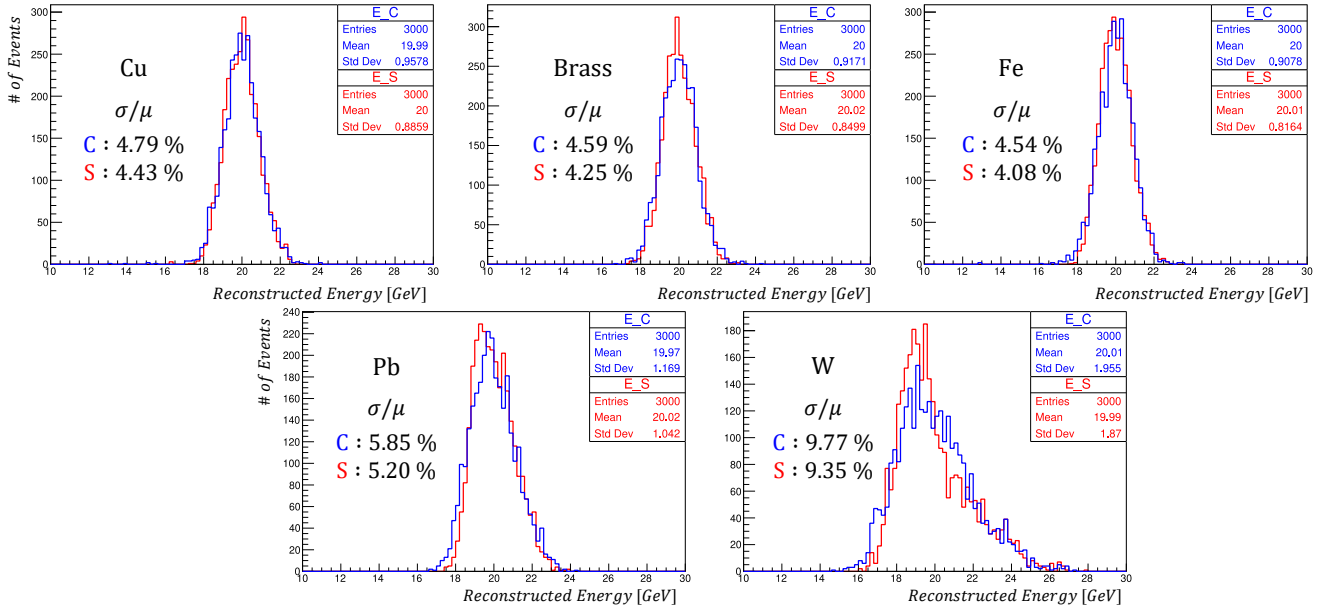
Figure 2. Reconstructed energy distribution of 20 GeV electrons on different absorbers, Cherenkov (blue) and scintillation (red) channel. The impact point dependence affects highly on resolution, especially for the absorbers with high Z value having long tail.

2.2 Calibration

To determine the detector's energy scale, calibration was done for all 5 absorber geometries. Calibration constant were derived using events of 20 GeV electron, matching signals from both the Cherenkov and scintillation channels to the total energy deposited in the detector. After calculating the calibration constants, the distribution of reconstructed energy was scaled to match the incoming particles' energy. This calibration is valid not only for EM particles but also for hadronic particles due to the unique feature of dual-readout calorimeter.

# of p.e. / GeV	Cu	Brass	Fe	Pb	W
Scintillation	1130	1180	1240	1000	600
Cherenkov	73	77	81	57	35

Table 1. Calculated average light yield of five different absorbers, with 20 GeV electron events. The unit is (number of photoelectrons)/(GeV).

During the calibration process, light yield - the inverse of calibration constant - was also calculated. Table 1 presents the average light yield for different absorbers. Generally, light yield is dependent on absorber's Z value; higher Z-values result in increased energy deposition within the absorber, reducing light yield. This difference in light yield significantly impacts the energy resolution of EM particles, as discussed in the next section.

3 Response to Electron

3.1 Energy Resolution

The EM energy performance of different absorbers were calculated with 5, 10, 20, 30, 50, 70, 90, 110 GeV elec-

tron events. The incident beam particles were directed toward the front center of the module, with a beam size of $10 \times 10 \ mm^2$ and initial angle of $(\theta, \phi) = (1.5°, 1.0°)$. For each energy point, 3000 events were generated.

Figure 2 illustrates the reconstructed energy distribution of 20 GeV electrons. Both channels have nearly identical sampling structures, resulting in a minimal difference in energy resolution primarily due to light yield fluctuations. Cu, Brass, and Fe (top three) exhibit well established gaussian distributions, while Pb and W (bottom two) results have a tail in the high energy region. This tail arises from the impact point dependence of the response [4]. Generally, as the Z value of absorber increases, the radiation length decreases, making the shower more compact and signal is dominated by response near the impact point. This dependence worsens energy resolution, especially for Pb and W.

The energy linearity, despite impact point dependency of response, still shows to be constant. Regardless of the absorber or energy points, linearity matches in ±1% to incoming beam energy.

The resolution of each energy point is calculated with the average and RMS of gaussian fit function applied to reconstructed energy distributions of Cherenkov, scintillation, and summation (C+S) channel - except W, that values of the distribution itself are used. Figure 3 shows an energy resolution by beam energy, fit energy points through stochastic and constant terms. Absorbers having relatively low Z values - Cu, Brass, and Fe - have stochastic term of summation channel to be under 12% and constant term near 0.1%. However, in case of high Z value absorbers - Pb and W -, stochastic term is generally worse (Pb : 12.7%, W : 14.1%) and especially constant term is large (Pb : 0.3%, W : 2.0%). This is due to the impact

point dependency of response, and relatively large fluctuation from their sampling structure and poor light yield, as shown previously.
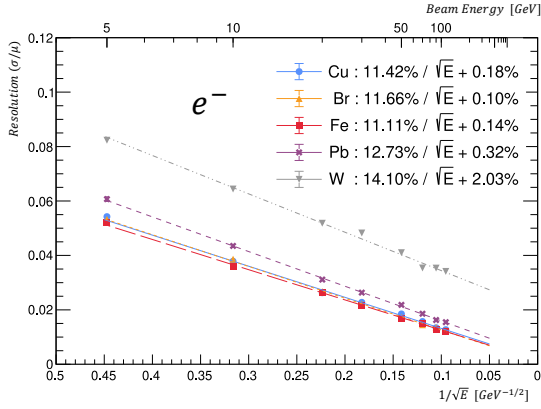

Figure 3. Summation (C+S) channel energy resolution of electrons on different absorbers.

3.2 Timing Resolution

One another significant feature that can be calculated from electron results is timing resolution. The optical physics inside the fiber is fully simulated, so timing structure of single event could be precisely calculated. Timing distribution of total events was obtained by calculating leading edge of single event timing distribution. The σ value of total timing distribution is referred to timing resolution of the geometry.

Similar to energy resolution, events of 20 GeV electrons with an identical initial angle were used. We scanned a range of leading edge percentage, from 5% to 100% (peak), investigated the fluctuation of timing resolution. In low percentage (under 50%), resolution of both channel less fluctuate and be minimum. However, as percentage increase, resolution get worse, especially in scintillation channel. The scintillation process, different from Cherenkov, has absorption and re-emission processes which make a fluctuation near the peak time. This fluctuation affects calculating leading edge near the peak, bring about a long tail on gaussian distribution of total timing.

Channel	Cu	Brass	Fe	Pb	W
Scintillation (ps)	71.2	70.9	78.5	56.9	59.9
Cherenkov (ps)	60.9	65.6	71.2	53.3	55.7

Table 2. Average timing resolution calculated using 30% leading edge point. Each value has ± 1 ps uncertainty.

Table 2 shows the average of calculated timing resolution, with 30% leading edge result. In contrast to energy resolution, timing resolution of absorbers shows opposite trend between absorbers having high/low Z value. As Z value of absorber increases, the shower and its timing distribution get more compact, resulting in better timing resolution.

4 Response to Charged Pion

4.1 (h/e) Calculation

The primary goal of the dual-readout calorimeter is the accurate measurement of hadronic showers by utilizing complementary information from Cherenkov and scintillation channels. To reconstruct the initial energy of hadronic particles, the ratio of hadronic to electromagnetic responses (h/e) for both channels must be calculated [1].

Prior to this calculation, attenuation correction was applied to the calibrated energy, as the simulation fully describes optical physics inside fiber, including absorption within the fibers. Using single-charged pion events, the depth of maximum shower was determined for each event using timing information. By fitting reconstructed energy as a function of depth, the attenuation length of optical fiber was calculated. Attenuation length is consistent across absorbers, so applied single value to all absorbers. Since attenuation length of Cherenkov channel (~ 11.99 m) was relatively longer than scintillation channel (~ 7.55 m) and negligible comparing the length of module, attenuation correction was applied only for scintillation channel.
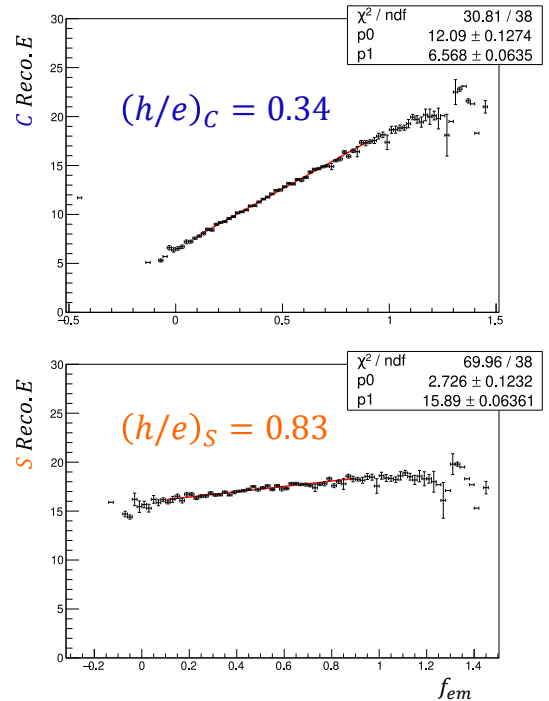

Figure 4. Reconstructed energy of Cherenkov (a) and scintillation (b) channel as a function of fraction of EM shower calculated by Eq. 1. Copper geometry, 20 GeV π^- result.

$$f_{EM} = \frac{(h/e)_C - (C/S)(h/e)_S}{(C/S)[1 - (h/e)_S] - [1 - (h/e)_C]} \quad (1)$$

Now the energy of hadronic particle is well reconstructed in both channels, giving different responses to same event. The (h/e) of each absorber geometry is calculated by scanning the (h/e) value of each Cherenkov and scintillation channel, finding the value that makes best

matching of reconstructed energy and initial beam energy at $f_{EM} = 1$. Figure 4 shows one (final) attempt of scanning process. The x-axis refers to f_{EM}, which can be calculated by the fact that (h/e) of Cherenkov and scintillation channel is different, using Eq. 1, where C,S refers to reconstructed energy of each channel. At $f_{EM} = 1$, since the calibration is done with electron, reconstructed energy of both channels must match to initial beam energy.

$$\chi = \frac{1 - (h/e)_S}{1 - (h/e)_C}, \quad \text{and} \quad E = \frac{S - \chi C}{1 - \chi} \quad (2)$$

Inserting obtained (h/e) values gives χ, which is the single factor needed for the dual-readout correction and represents the geometry. Finally Eq. 2 completes the dual-readout correction, reconstructing the energy of initial beam particle as figure 5.
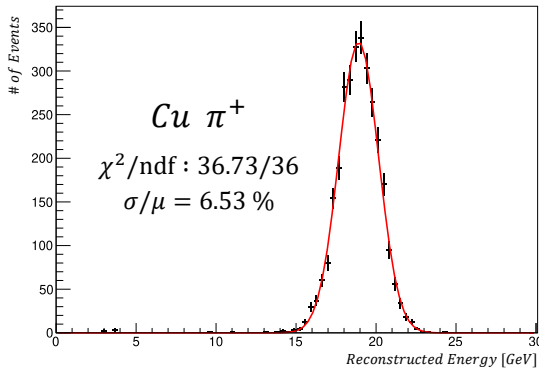

Figure 5. Distribution of dual-readout corrected energy of 20 GeV charged pion, on copper geometry. The distribution well establish gaussian.

4.2 Energy Resolution

After obtaining χ value of each geometry, now the hadronic energy response was evaluated. Used single charged pion (π^+) events with energies ranging from 5 GeV to 110 GeV, with all other conditions same as electron case.

Unlike electrons, due to the fact that f_{em} increases as energy does, energy response to pion shows a nonlinear increase on both Cherenkov and scintillation channels. Despite this, dual-readout corrected energy yield a constant response, regardless of energy points or absorber. Yet, for low Z absorbers, the corrected energy is somewhat ($\simeq 5\%$) lower than the initial beam energy, which is one of the discrepancies between the real experiment and GEANT4 simulation.

Figure 6 shows the energy resolution of a single charged pion, after dual-readout correction. Relatively low Z absorbers still give competitive performance compared to heavy absorbers, having resolution under 4% for 110 GeV π^- and stochastic term under 30% of dual-readout corrected energy. In case of tungsten, there is no significant difference between scintillation and dual-readout corrected channel, since the compensation is nearly achieved (h/e=0.99).

In spite of the discrepancy between the real experiment result and GEANT4 simulation, the characteristics of core results - such as nonlinear increase of response on energy increase - are well described. These features allow us to conclude that low Z absorbers are still attractive choices in perspective of hadronic response.
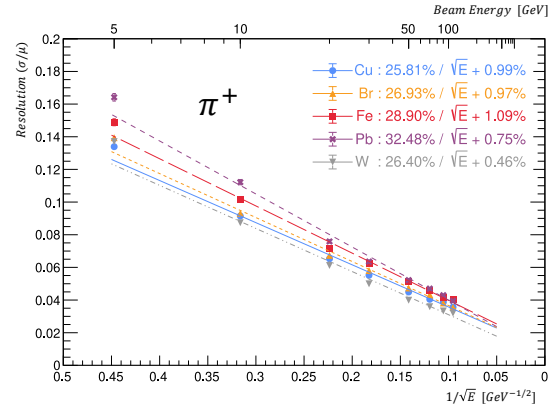

Figure 6. Dual-readout corrected energy resolution of charged pions on different absorbers. Stochastic(constant) term fluctuates under $\pm 2\%(\pm 0.2\%)$ on different energy fitting range.

5 Summary

Based on MC simulations, we studied the performance of dual-readout calorimeter with various absorbers. For electrons, energy resolution worsens with increasing Z-value, whereas timing resolution improves. For charged pions, low Z-value absorbers demonstrated competitive performance, achieving stochastic terms below 30%, while tungsten was found to be incompatible with the dual-readout method due to limited compensation.

Considering both EM and hadronic performance, if the energy deposit is ensured, low Z-value absorbers such as copper, brass, and iron present an advantage in terms of energy resolution, making them suitable candidates for dual-readout calorimeter designs.

References

[1] L. Sehwook, L. Michele, W. Richard, Rev. Mod. Phys. **90**, 025002 (2018). https://link.aps.org/doi/10.1103/RevModPhys.90.025002

[2] S. Agostinelli, *et al*, Nucl. Instrum. Meth. A **506**, 250-303 (2003). https://doi.org/10.1016/S0168-9002(03)01368-8

[3] Hamamatsu Photonics, S13615-1025N MPPCs in a chip size package miniaturized through the adoption of TSV structure, https://www.hamamatsu.com/content/dam/hamamatsu-photonics/sites/documents/99_SALES_LIBRARY/ssd/s13615_series_kapd1062e.pdf

[4] N. Akchurin, *et al*, Nucl. Instrum. Meth. A **762**, 100-118 (2014). https://doi.org/10.1016/j.nima.2014.05.121